J|A|C|S
ARTICLES

Published on Web 06/14/2008

NMR Studies of Ultrafast Intramolecular Proton Tautomerism in Crystalline and Amorphous *N,N′*-Diphenyl-6-aminofulvene-1-aldimine: Solid-State, Kinetic Isotope, and Tunneling Effects

Juan Miguel Lopez del Amo,[†] Uwe Langer,[†] Verónica Torres,[†] Gerd Buntkowsky,[‡] Hans-Martin Vieth,[§] Marta Pérez-Torralba,[||] Dionísia Sanz,[||] Rosa María Claramunt,[||] José Elguero,[⊥] and Hans-Heinrich Limbach*,[†]

Institut für Chemie and Biochemie, Takustrasse 3, Freie Universität Berlin, D-14195 Berlin, Germany, Institut für Experimentalphysik, Arnimallee 14, Freie Universität Berlin, D-14195 Berlin, Germany, Institut für Physikalische Chemie der Friedrich-Schiller Universität, Helmholtzweg 4, D-07743 Jena, Germany, Departamento de Química Orgánica and Bio-Orgánica, Facultad de Ciencias, Universidad Nacional de Educación a Distancia, Senda del Rey 9, E-28040 Madrid, Spain, and Centro de Química Orgánica Manuel Lora-Tamayo, CSIC, Juan de la Cierva 3, E-28006, Madrid, Spain

Received February 28, 2008; E-mail: limbach@chemie.fu-berlin.de

Abstract: Using solid-state NMR spectroscopy, we have detected and characterized ultrafast intramolecular proton tautomerism in the N−H−N hydrogen bonds of solid *N,N′*-diphenyl-6-aminofulvene-1-aldimine (**I**) on the microsecond-to-picosecond time scale. ^{15}N cross-polarization magic-angle-spinning NMR experiments using ^{1}H decoupling performed on polycrystalline **I**-$^{15}N_2$ and the related compound *N*-phenyl-*N′*-(1,3,4-triazole)-6-aminofulvene-1-aldimine (**II**) provided information about the thermodynamics of the tautomeric processes. We found that **II** forms only a single tautomer but that the gas-phase degeneracy of the two tautomers of **I** is lifted by solid-state interactions. Rate constants, including H/D kinetic isotope effects (KIEs), on the microsecond-to-picosecond time scale were obtained by measuring and analyzing the longitudinal ^{15}N and ^{2}H relaxation times of **I**-$^{15}N_2$, **I**-$^{15}N_2$-d_{10}, and **I**-$^{15}N_2$-d_1 over a wide temperature range. In addition to the microcrystalline modification, a novel amorphous modification of **I** was found and studied. In this modification, proton transfer is much faster than in the crystalline form. For both modifications, we observed large H/D KIEs that were temperature-dependent at high temperatures and temperature-independent at low temperatures. These findings are interpreted in terms of a simple quasiclassical tunneling model proposed by Bell and modified by Limbach. We obtained evidence that a reorganization energy is necessary in order to compress the N−H−N hydrogen bond and achieve a molecular configuration in which the barrier for H transfer is reduced and tunneling or an over-barrier reaction can occur.

Introduction

Kinetic isotope effects (KIEs) in hydrogen-transfer reactions generally depend on temperature, a phenomenon which has been explained by Bigeleisen[1] in terms of a combination of Eyring's transition-state theory[2] and isotope-fractionation theory. This temperature dependence arises mainly from a difference in the zero-point energies of the initial and the transition states. As Bell has shown,[3] tunneling through the reaction barrier enhances KIEs at high temperatures but can lead to temperature-independent rate constants and KIEs at low temperatures. However, if the H transfer is preceded by fast motions of major heavy atoms, such as in hydrogen-bond equilibria[4] or conformational changes,[5] or constitutes an uphill reaction,[6,7] temperature-independent KIEs combined with temperature dependence of the rate constants can be observed. In this case, a minimum free energy is required in order for "ground state" tunneling

[†] Institut für Chemie and Biochemie, Freie Universität Berlin.
[‡] Friedrich-Schiller Universität.
[§] Institut für Experimentalphysik, Freie Universität Berlin.
[||] Universidad Nacional de Educación a Distancia.
[⊥] CSIC.

(1) (a) Bigeleisen, J. *J. Chem. Phys.* **1949**, *17*, 675–678. (b) Bigeleisen, J. *J. Chem. Phys.* **1955**, *23*, 2264–2267. (c) Melander, L.; Saunders, W. H. *Reaction Rates of Isotopic Molecules*; Krieger: Malabar, FL, 1987.
(2) Glasstone, S.; Laidler, J.; Eyring, H. *The Theory of Rate Processes*; McGraw-Hill: New York, 1941.
(3) (a) Bell, R. P. *The Proton in Chemistry*, 2nd ed.; Chapman and HalI: London, 1973. (b) Bell, R. P. *The Tunnel Effect*; Chapman and Hall: London, 1980.
(4) (a) Gerritzen, D.; Limbach, H.-H. *J. Am. Chem. Soc.* **1984**, *106*, 869–879. (b) Limbach, H. H.; Klein, O.; López del Amo, J. M.; Elguero, J. *Z. Phys. Chem.* **2004**, *217*, 17–49.
(5) Limbach, H.-H.; Lopez, J. M.; Kohen, A. *Philos. Trans. R. Soc. London* **2006**, *B361*, 1399–1415.
(6) (a) Braun, J.; Schlabach, M.; Wehrle, B.; Köcher, M.; Vogel, E.; Limbach, H.-H. *J. Am. Chem. Soc.* **1994**, *116*, 6593–6604. (b) Braun, J.; Limbach, H.-H.; Williams, P. G.; Morimoto, H.; Wemmer, D. *J. Am. Chem. Soc.* **1996**, *118*, 7231–7232.
(7) Limbach, H.-H. In *Hydrogen Transfer Reactions*; Hynes, J. T., Klinman, J., Limbach, H.-H., Schowen, R. L. Eds.; Wiley-VCH: Weinheim, Germany, 2007; Vols. *1&2*, Chapter 6, pp 135−221, and references cited therein.

 10.1021/ja801506n CCC: $40.75

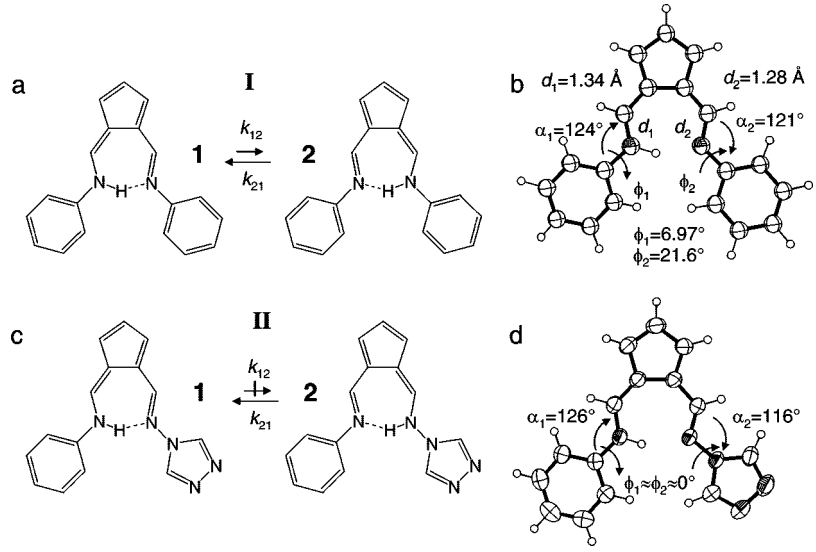

Figure 1. Tautomerism in (a) **I** and (c) **II** and X-ray structures of (b) **I**[31]and (d) **II**.[27]

arising from the heavy-atom reorganization to occur. This term corresponds to the "work term" in the Marcus theory of electron transfer.[8] Temperature-independent KIEs have been observed in recent years for a number of hydrogen tunneling reactions in enzymes.[9–12] Arrhenius curves for such H transfers can be described in terms of quasiclassical tunneling models such as the Dogonatze−Kusnetzov−Ulstrup model[10,13] or in terms of a modified Bell model.[4,5,7] The description of Arrhenius curves using first principles is more desirable but also much more difficult.[14–16]

In order to further develop the theory of H transfer from kinetic studies, kinetic data over a wide temperature range are required; these data are difficult to obtain for liquid solutions, particularly in the case of enzymes in water. In contrast, kinetic data can be obtained more easily in the case of model systems in the solid state. Especially important are degenerate or quasidegenerate reversible systems, which are preferentially studied using dynamic NMR spectroscopy. Using this method, some of us have studied model systems involving double, triple, and quadruple proton transfers,[4,5,7,17–19] which are generally slower and hence more easily studied than single proton transfers; in addition, a solid-state single proton transfer has been monitored.[20] Traditionally, dynamic NMR spectroscopy is well-suited for following reactions on the second-to-microsecond time scale, but the development of solid-state longitudinal-relaxation NMR techniques under high-resolution[19,21–23] and/or field-cycling conditions[24,25] has extended this regime to the microsecond-to-nanosecond time scale.

The aim of this paper is to present the results of a combined solid-state ^{1}H, ^{2}H, and ^{15}N NMR study in which the H/D KIEs of an ultrafast H transfer in the N−H−N hydrogen bonds of a model system have been obtained across very large temperature and dynamic ranges. The model solid is the H chelate *N*,*N*′-diphenyl-6-aminofulvene-1-aldimine (**I**) (Figure 1a,b). It has been well-known for a long time that this molecule exhibits a degenerate proton tautomerism both in the gas phase and in solution; however, this process could not be followed using any

(8) Marcus, R. A. *J. Chem. Phys.* **1966**, *45*, 4493–4499.
(9) Knapp, M. J.; Rickert, K.; Klinman, J. P. *J. Am. Chem. Soc.* **2002**, *124*, 3865–3874.
(10) Kohen, A.; Cannio, R.; Bartolucci, S.; Klinman, J. P. *Nature* **1999**, *399*, 496–499.
(11) Kohen, A. In *Isotope Effects in Chemistry and Biology*; Kohen, A., Limbach, H.-H. Eds.; Taylor & Francis: Boca Raton, FL, 2006; Chapter 28, pp 743−765.
(12) (a) Basran, J.; Patel, S.; Sutcliffe, M. J.; Scrutton, N. S. *J. Biol. Chem.* **2001**, *276*, 6234–6242. (b) Basran, J.; Masgrau, L.; Sutcliffe, M. J.; Scrutton, N. S. In *Isotope Effects in Chemistry and Biology*; Kohen, A., Limbach, H.-H. Eds.; Taylor & Francis: Boca Raton, FL, 2006; Chapter 25, pp 671−690.
(13) (a) Kuznetsov, A. M.; Ulstrup, J. *Can. J. Chem.* **1999**, *77*, 1085–1096. (b) Kuznetsov, A. M.; Ulstrup, J. In *Isotope Effects in Chemistry and Biology*; Kohen, A., Limbach, H.-H. Eds.; Taylor & Francis: Boca Raton, FL, 2006; Chapter 26, pp 691−724.
(14) Truhlar, D. In *Isotope Effects in Chemistry and Biology*; Kohen, A., Limbach, H.-H. Eds.; Taylor & Francis: Boca Raton, FL, 2006; Chapter 22, pp. 579−620.
(15) Smedarchina, Z.; Siebrand, W.; Fernández-Ramos, A. In *Isotope Effects in Chemistry and Biology*; Kohen, A., Limbach, H.-H. Eds.; Taylor & Francis: Boca Raton, FL, 2006; Chapter 20, pp 521−548.
(16) Brackhagen, O.; Scheurer, C.; Meyer, R.; Limbach, H.-H. *Ber. Bunsenges. Phys. Chem.* **1998**, *102*, 303–316.
(17) (a) Aguilar-Parrilla, F.; Scherer, G.; Limbach, H.-H.; Foces-Foces, M. C.; Cano, F. H.; Smith, J. A. S.; Toiron, C.; Elguero, J. *J. Am. Chem. Soc.* **1992**, *114*, 9657–9659. (b) Aguilar-Parrilla, F.; Limbach, H.-H.; Foces-Foces, C.; Cano, F. H.; Jagerovic, N.; Elguero, J. *J. Org. Chem.* **1995**, *60*, 1965–1970. (c) Aguilar-Parrilla, F.; Klein, O.; Elguero, J.; Limbach, H.-H. *Ber. Bunsenges. Phys. Chem.* **1997**, *101*, 889–901. (d) Klein, O.; Bonvehi, M. M.; Aguilar-Parrilla, F.; Elguero, J.; Limbach, H.-H. *Isr. J. Chem.* **1999**, *34*, 291–299.
(18) Klein, O.; Aguilar-Parrilla, F.; Lopez, J. M.; Jagerovic, N.; Elguero, J.; Limbach, H.-H. *J. Am. Chem. Soc.* **2004**, *126*, 11718–11732.
(19) Lopez, J. M.; Männle, F.; Wawer, I.; Buntkowsky, G.; Limbach, H.-H. *Phys. Chem. Chem. Phys.* **2007**, *9*, 4498–4513.
(20) (a) Braun, J.; Hasenfratz, C.; Schwesinger, R.; Limbach, H.-H. *Angew. Chem.* **1994**, *106*, 2302–2304. (b) Braun, J.; Hasenfratz, C.; Schwesinger, R.; Limbach, H.-H. *Angew. Chem., Int. Ed. Engl.* **1994**, *33*, 2215–2217. (c) Braun, J.; Schwesinger, R.; Williams, P. G.; Morimoto, H.; Wemmer, D. E.; Limbach, H.-H. *J. Am. Chem. Soc.* **1996**, *118*, 11101–11110.
(21) Hoelger, C. G.; Wehrle, B.; Benedict, H.; Limbach, H.-H. *J. Phys. Chem.* **1994**, *98*, 843–851.
(22) Langer, U.; Latanowicz, L.; Hoelger, C.; Buntkowsky, G.; Vieth, H. M.; Limbach, H.-H. *Phys. Chem. Chem. Phys.* **2001**, *3*, 1446–1458.
(23) (a) Limbach, H.-H. In *NMR Basic Principles and Progress*; Springer-Verlag: Heidelberg, Germany, 1991; Vol. 23, pp 66−167. (b) Limbach, H.-H. In *Advances in NMR*; Grant, D. M., Harris, R. K. Eds.; Encyclopedia of Nuclear Magnetic Resonance, Vol. 9; Wiley: Chichester, U.K., 2002; pp 520−531.
(24) Xue, Q. A.; Horsewill, A. J.; Johnson, M. R.; Trommsdorff, H. P. *J. Chem. Phys.* **2004**, *120*, 11107–11119.
(25) Brougham, D. F.; Caciuffo, R.; Horsewill, A. J. *Nature* **1999**, *397*, 241–243.

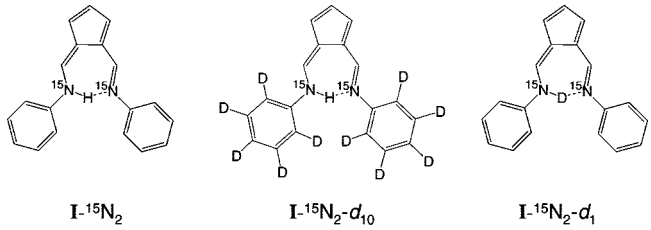

Figure 2. Isotopologues of **I** used in this study.

kinetic method.[26] The geometries of the hydrogen bonds of **I** and the asymmetrically substituted analog *N*-phenyl-*N*′-(1,3,4-triazole)-6-aminofulvene-1-aldimine (**II**) (Figure 1c,d) in solution as well as those of other derivatives have been characterized by the observation and interpretation of the scalar $^{15}N-H$, $H-^{15}N$, and $^{15}N-^{15}N$ couplings across the $^{15}N-H-^{15}N$ hydrogen bonds of the ^{15}N-labeled compounds.[27–29] The latter couplings in 6-aminofulvene-1-aldimines have been also obtained recently using solid-state NMR.[30] To our knowledge, NMR studies of the solid-state tautomerism of **I** have not been performed to date. Here we show that the proton tautomerism is also present in the solid state, although the gas-phase degeneracy is lifted by intermolecular interactions. Using various relaxation techniques, we determined the H/D KIEs for **I** over a very wide temperature range, in which the KIE was observed to switch from a temperature-dependent to a temperature-independent regime. In addition to the known crystalline form[31] of **I**, we also observed an amorphous form whose H-transfer characteristics differ substantially from those of the crystalline form. Whereas we observed a fast, quasidegenerate H transfer in **I**, no dynamics could be detected for **II**.

In particular, we proceeded as follows. Doubly ^{15}N-labeled **I** was synthesized, and its high-resolution solid-state ^{15}N NMR spectra with cross-polarization (CP), ^1H decoupling, and magic-angle spinning (MAS) were obtained. These spectra gave information about the thermodynamics of the quasidegenerate H transfer. The measurement of the longitudinal ^{15}N T_1 relaxation times provided initial information about the kinetics. However, as MAS is difficult at low temperatures, we followed the H transfer using ^2H T_1 relaxation time measurements of **I**-$^{15}N_2$-d_{10} deuterated on the phenyl rings, as we found that these deuterons are subject to dipolar relaxation caused by the mobile proton. ^1H T_1 relaxation time measurements of **I**-$^{15}N_2$-d_{10} were less informative. The kinetics of the D transfer was followed by measuring the longitudinal ^2H relaxation times of **I**-$^{15}N_2$-d_1 deuterated at the mobile proton site. All three isotopologues of **I** are depicted in Figure 2.

This paper is organized as follows. After the Experimental Section, the thermodynamic and kinetic results observed for the crystalline and amorphous forms of **I** will be detailed. Following that, the collected kinetic data obtained for the H and D transfers will be plotted in Arrhenius diagrams fitted using the Bell−Limbach model, and finally, the results of the work will be discussed.

Table 1. Isotopically Labeled Samples of Crystalline and Amorphous **I** and the Measurements in Which They Were Used

sample	crystallinity (%)	NMR method used
I -$^{15}N_2$-c	100	variable-temperature ^{15}N NMR and ^{15}N T_1
I-$^{15}N_2$-d_{10}-c	100	variable-temperature ^2H T_1 and ^1H T_1
I-$^{15}N_2$-d_1-c	100	variable-temperature ^2H T_1
I-$^{15}N_2$-d_{10}-a*	20	variable-temperature ^{15}N NMR
I-$^{15}N_2$-d_{10}-a	<10	variable-temperature ^2H T_1
I-$^{15}N_2$-d_1-a	<10	variable-temperature ^2H T_1

Experimental Section

Sample Preparation. **I**-$^{15}N_2$ and **I**-$^{15}N_2$-d_{10} were prepared using ^{15}N-labeled aniline enriched to 95% with ^{15}N and ^{15}N-labeled aniline-d_5, respectively, as described previously.[27] These compounds were synthesized as described previously,[32] using $NH_4{}^{15}NO_3$ as an ^{15}N source. Because of the small amounts of isotopically labeled **I** resulting from this synthesis, no further purification was performed, although the liquid ^1H NMR spectrum as well as the low-temperature solid-state ^{15}N NMR spectra showed a small impurity.

Deuteration of **I** at the mobile proton site was achieved by dissolving the sample three times in methanol-d_1 (Sigma-Aldrich) and evaporating the solvent under vacuum.

The amorphous form of **I** was obtained by dissolving a sample in the minimum possible amount of warm methanol (or methanol-d_1 for **I**-$^{15}N_2$-d_1) and then immediately decreasing the temperature to −20 °C. After only a few minutes, almost all of the compound was precipitated. The sample obtained by this procedure had spectroscopic properties in agreement with an amorphous structure, as discussed below.

The different samples investigated in this study are characterized in Table 1. Polycrystalline samples are labeled with "c" and amorphous samples with "a". Samples were considered to be amorphous when the microcrystalline content was less than 10%. The index "a*" refers to a sample with a crystalline content of 20%. The different grades of crystallinity were calculated on the basis of ^{15}N NMR line-shape analysis, as discussed below.

NMR Spectroscopy. The ^{15}N CPMAS spectra were recorded at 9.12 and 30.12 MHz using Bruker CXP 100 and MSL 300 NMR spectrometers equipped with standard 7 mm and 5 mm Doty probeheads. We used a normal cross-polarization sequence (which minimizes ringing artifacts[33]) with cross polarization times of 3 to 8 ms, ^1H 90° pulse widths of 6−10 μs, and recycle delays of 3−10 s. For measurements of the ^{15}N longitudinal relaxation times (T_1) in connection with the CP scheme, a pulse sequence described by Torchia[34] was employed. As a result of phase cycling of the first proton 90° pulse and the receiver phase, the accumulated magnetizations in this experiment cancel at longer mixing times; this contrasts with the most frequently applied inversion−recovery pulse sequence, where the equilibrium magnetization approaches maximum intensity. Between 500 and 2500 scans were accumulated on average, with a contact time for cross-polarization of 1.5−5.0 ms and a repetition time of 1−3 s. Low-temperature measurements were carried out by passing nitrogen gas through a home-built heat exchanger[35] immersed in liquid nitrogen, which allowed temperatures as low as 90 K to be achieved while maintaining spinning speeds between 2 and 2.5 kHz, which are large enough to produce

(26) Mueller-Westerhoff, U. *J. Am. Chem. Soc.* **1970**, *92*, 4849.
(27) (a) Claramunt, R. M.; Sanz, D.; Alarcón, S. H.; Pérez-Torralba, M.; Elguero, J.; Foces-Foces, C.; Pietrzak, M.; Langer, U.; Limbach, H.-H. *Angew. Chem.* **2001**, *113*, 434–437. (b) Claramunt, R. M.; Sanz, D.; Alarcón, S. H.; Pérez-Torralba, M.; Elguero, J.; Foces-Foces, C.; Pietrzak, M.; Langer, U.; Limbach, H.-H. *Angew. Chem., Int. Ed.* **2001**, *40*, 420–423.
(28) Pietrzak, M.; Limbach, H.-H.; Perez-Torralba, M.; Sanz, D.; Claramunt, R. M.; Elguero, J. *Magn. Reson. Chem.* **2001**, *39*, S100–S108.
(29) Sanz, D.; Pérez-Torralba, M.; Alarcón, S. H.; Claramunt, R. M.; Foces-Foces, C.; Elguero, J. *J. Org. Chem.* **2002**, *67*, 1462–1471.
(30) (a) Brown, S. P.; Perez-Torralba, M.; Sanz, D.; Claramunt, R. M.; Emsley, L. *Chem. Commun.* **2002**, 1852–1853. (b) Brown, S. P.; Perez-Torralba, M.; Sanz, D.; Claramunt, R. M.; Emsley, L. *J. Am. Chem. Soc.* **2002**, *124*, 1152–1153.
(31) Ammon, H. L.; Müller-Westerhoff, U. *Tetrahedron* **1974**, *30*, 1437–1443.
(32) Otting, H.; Rumpel, L.; Meschede, G.; Scherer, G.; Limbach, H.-H. *Ber. Bunsenges. Phys. Chem.* **1986**, *90*, 1122–1129.
(33) Murphy, P. D. B. *J. Magn. Reson.* **1986**, *70*, 307–312.
(34) Torchia, D. *J. Magn. Reson.* **1978**, *30*, 613–616.
(35) Kendrick, R. D.; Friedrich, S.; Wehrle, B.; Limbach, H.-H.; Yannoni, C. S. *J. Magn. Reson.* **1985**, *65*, 159–161.

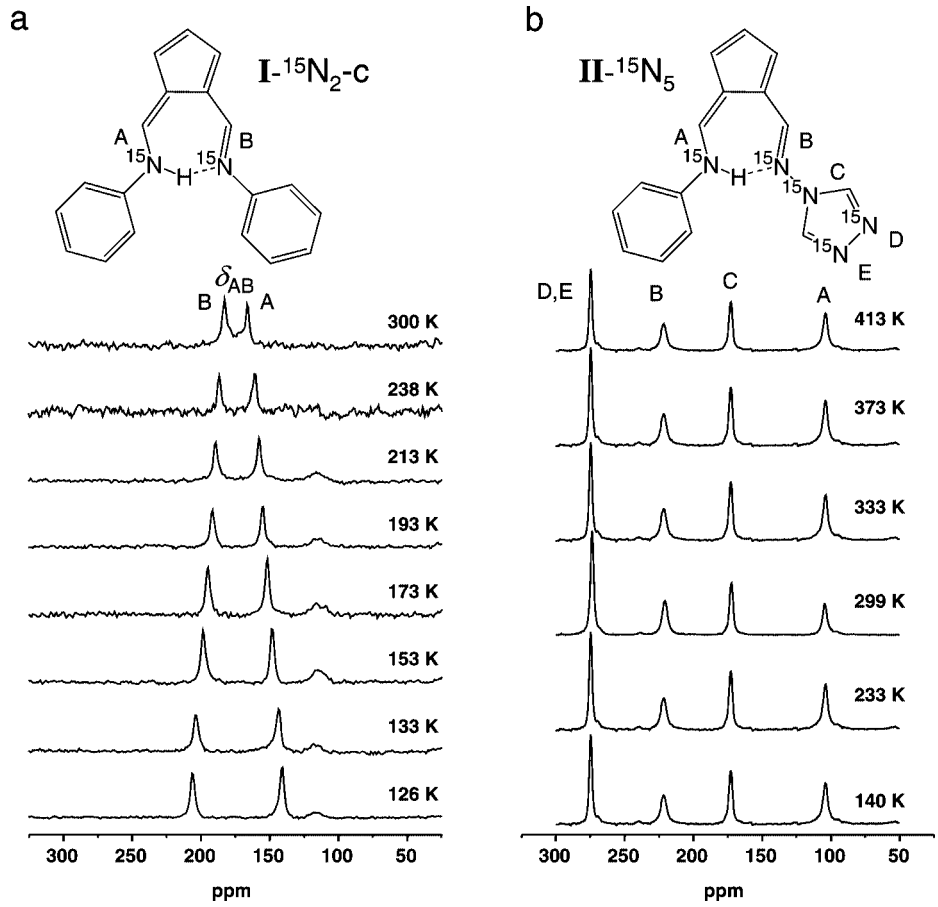

Figure 3. Variable-temperature 30.41 MHz ^{15}N CPMAS NMR spectra of polycrystalline (a) I−$^{15}N_2$-c and (b) **II**-$^{15}N_5$-c.

spectra that are essentially free of rotational sidebands. Chemical shifts were referenced to external solid $^{15}NH_4Cl$.

Measurements of the ^{2}H T_1 relaxation times of the deuterated samples were performed on a home-built 7 T spectrometer operating at a Larmor frequency of 46.03 MHz and equipped with a home-built low-temperature ^{2}H probe. The measurements employed a saturation−recovery pulse sequence followed by a solid-echo sequence and recording of the echo. The saturation part involved a string of 90° pulses (3.6 μs) with nonequal spacing to avoid formation of undesired echoes. The two 90° pulses of the solid-echo sequence were spaced by 35 μs. Finally, the echo was Fourier transformed, allowing the evaluation of T_1 for individual lines in the spectrum.

Results

Variable-Temperature ^{15}N CPMAS Spectroscopy and Thermodynamics of I. Variable-temperature ^{15}N CPMAS spectra of polycrystalline **I**-$^{15}N_2$ are shown in Figure 3a. At room temperature, two lines (at 184 and 167 ppm) were observed, indicating that the two nitrogen atoms are nonequivalent. When the temperature was decreased to 126 K, the splitting between the two lines (now at 207 ppm and 141 ppm) increased. No coalescence was found anywhere in the temperature range. This result can be explained by the presence of a slightly asymmetric double-well potential for proton motion, as proposed previously.[22,36–38] This means that the gas-phase degeneracy of the two tautomeric states was removed as a result of intermolecular interactions in the solid. The small broad line at 118 ppm observed below 220 K, which was also seen in the ^{1}H liquid NMR spectrum (not shown), were assigned to an impurity. All of the chemical shifts and line separations are summarized in Table S1 in the Supporting Information.

In contrast, the corresponding spectra of polycrystalline **II**-$^{15}N_5$-c (shown in Figure 3b) did not show any dependence on temperature. The signal assignment proposed is straightforward and based on liquid-state NMR studies.[27]

The averaged ^{15}N chemical shifts of **I**-$^{15}N_2$-c are given by[36,37]

$$\delta_A = \frac{1}{1+K_{12}}\Delta_A + \frac{K_{12}}{1+K_{12}}\Delta_B, \quad \delta_B = \frac{K_{12}}{1+K_{12}}\Delta_A + \frac{1}{1+K_{12}}\Delta_B \quad (1)$$

where K_{12} represents the equilibrium constant for the proton tautomerism and δ_i and Δ_i the averaged and intrinsic chemical shifts of nucleus i. It follows from eq 1 that

$$\tfrac{1}{2}(\delta_A + \delta_B) = \tfrac{1}{2}(\Delta_A + \Delta_B) \quad (2)$$

and that

$$\delta_{AB} = \Delta_{AB}\frac{1-K_{12}}{1+K_{12}} \quad (3)$$

where $\delta_{AB} = \delta_B - \delta_A$ and $\Delta_{AB} = \Delta_B - \Delta_A$ are the averaged and intrinsic splittings, respectively. The equilibrium constant can be calculated from eq 3 and the averaged splitting δ_{AB} if

(36) Limbach, H.-H.; Hennig, J.; Kendrick, R.; Yannoni, C. S. *J. Am. Chem. Soc.* **1984**, *106*, 4059–4060.
(37) Wehrle, B.; Zimmermann, H.; Limbach, H.-H. *J. Am. Chem. Soc.* **1988**, *110*, 7014–7024.
(38) Wehrle, B.; Limbach, H.-H. *Chem. Phys.* **1989**, *136*, 223–247.

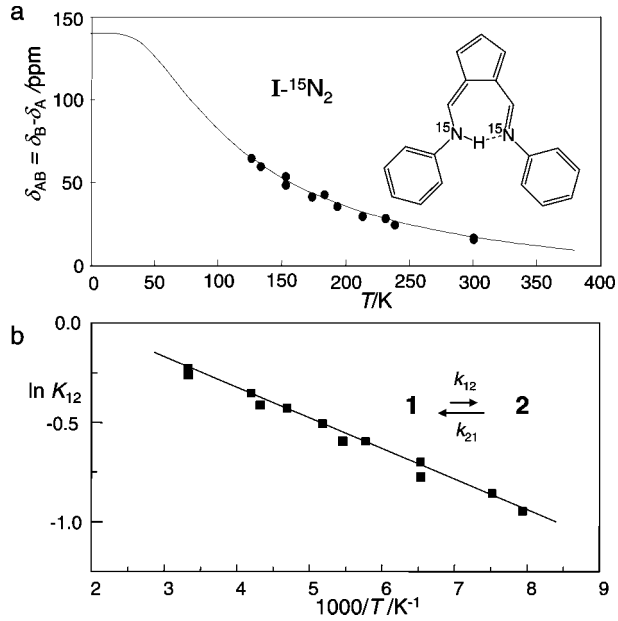

Figure 4. (a) Splitting of the two ^{15}N signals of polycrystalline **I**-$^{15}N_2$-c as a function of temperature and (b) the corresponding van't Hoff plot.

the intrinsic splitting Δ_{AB} is known. Since δ_{AB} continued to increase at low temperatures, Δ_{AB} could not be obtained directly. Therefore, we assumed that the value of Δ_A was similar to the value of 105 ppm found for the imino nitrogen of **II**-$^{15}N_5$-c. Using the experimental value of 174 ppm for $^1/_2(\delta_A + \delta_B)$, we then obtained from eq 2 a Δ_B value of 245 ppm, i.e., an intrinsic splitting Δ_{AB} of 140 ppm. In this way, we obtained the equilibrium constant values listed in Table S2 in the Supporting Information. They followed the van't Hoff equation given by eq 4:

$$K_{12} = \frac{k_{12}}{k_{21}} = \frac{x_2}{x_1} = \exp(0.3 - 165/T) = \exp\left(\frac{\Delta S_{12}}{R} - \frac{\Delta H_{12}}{RT}\right) \quad (4)$$

where k_{12} and k_{21} represent the forward and reverse rate constants, respectively, and x_1 and x_2 the mole fractions of the two tautomers. This equation yields a reaction enthalpy (ΔH_{12}) of 1.4 ± 0.1 kJ mol^{-1} and a reaction entropy (ΔS_{12}) of 2.49 ± 0.05 J mol^{-1} K^{-1}. The experimental and calculated temperature-dependent chemical-shift splittings are depicted in Figure 4a and the van't Hoff plot in Figure 4b.

The room-temperature ^{15}N CPMAS NMR spectrum of a sample of amorphous **I**-$^{15}N_2$-a is shown in Figure 5a. Lines A* and B* stem from the amorphous form and lines A and B from a small amount of the polycrystalline form. Within the margin of error, the positions of A* and B* coincide with those of A and B, respectively. In contrast, the line widths were much larger for the amorphous lines. Line-shape analysis was performed assuming Lorentzian lines, as depicted in Figure 5; the parameter values employed are assembled in Table S2 in the Supporting Information. The line broadening can be attributed to a distribution of local environments in the amorphous solid, giving rise to a distribution of equilibrium constants in a manner similar to that found previously for related systems.[37]

We estimated a crystallinity of 8% for the sample in Figure 5a. However, we noted that the crystalline fraction of the sample increased with time. After the sample was left for 2 months at room temperature, we obtained the spectra shown in Figure

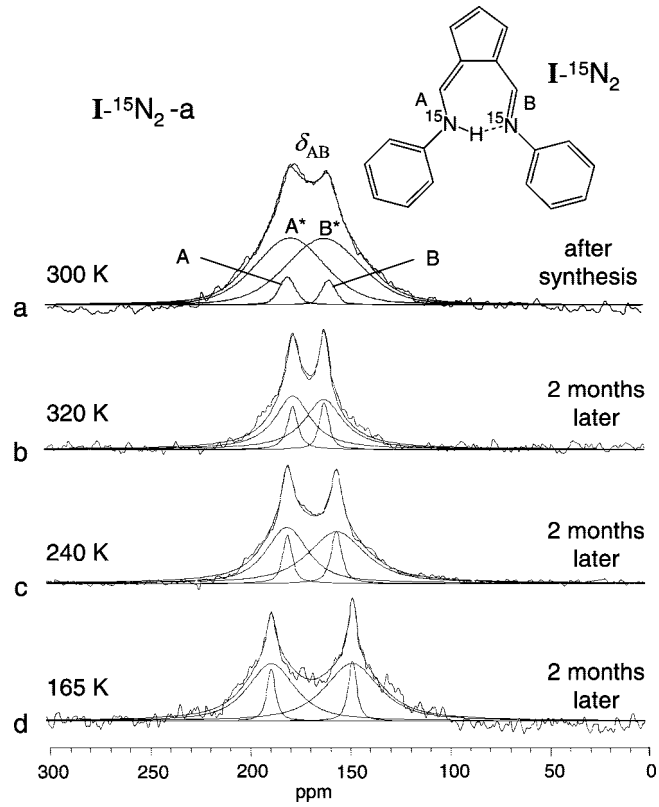

Figure 5. (a) ^{15}N spectra of a **I**-$^{15}N_2$-a sample measured at room temperature. Lines A and B correspond to the crystalline phase and broad lines A* and B* to the amorphous component. (b–d) ^{15}N-{^{1}H} CPMAS spectra of the same sample at various temperatures, measured 2 months after the spectrum in (a).

5b–d. At this point, line-shape analysis gave a crystalline fraction of 20%, indicating a slow rearrangement of the amorphous form to the more stable crystalline form. The low-temperature spectra showed that the splitting between the broad lines of the amorphous form increased in a manner similar to that of the polycrystalline form.

These results indicate that the hydrogen-bond asymmetry of the amorphous phase of **I** consists of a distribution of values that are on average equal to those observed in the microcrystalline sample. Thus, the average reaction enthalpy and entropy of the amorphous form are similar to those of the polycrystalline form.

^{15}N Longitudinal Relaxation Times of I-$^{15}N_2$-c. The fast proton tautomerism observed in solid **I** modulates the ^{15}N–H dipolar interaction, so in principle, the rate of proton transfer in **I** can be obtained by measuring the temperature dependence of the ^{15}N T_1 relaxation time, as shown previously.[21] Figure 6 shows a plot of T_1 (obtained at 9.12 MHz using a 2.1 T spectrometer) as a function of reciprocal temperature. The data are also listed in Table S3 in the Supporting Information. In contrast to the case for other systems,[21,39] the expected minimum in T_1 could not be reached at low temperatures because the H transfer is very fast. From the slope of the left portion of the predicted T_1 curve, a high-temperature activation energy of only 9 kJ mol^{-1} was obtained. In this situation, it was not easy to accurately determine the associated rate constants, as some

(39) Langer, U.; Hoelger, C.; Wehrle, B.; Latanowicz, L.; Vogel, E.; Limbach, H.-H. *J. Phys. Org. Chem.* **2000**, *13*, 23–34.

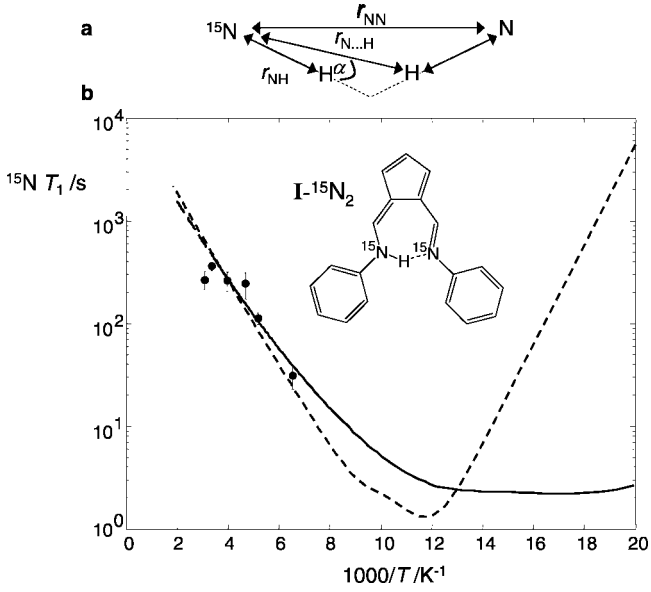

Figure 6. (a) Change of the hydrogen-bond geometry associated with the tautomerism of **I**; α is the jump angle of the dipolar ^{1}H−^{15}N interaction. (b) ^{15}N longitudinal relaxation times of polycrystalline **I**-$^{15}N_2$ measured at 2.1 T (9.12 MHz) as a function of reciprocal temperature. The dashed line was calculated using a simple Arrhenius law (eq 8), while the solid line was calculated using the rate constants for H tautomerism in crystalline **I**-$^{15}N_2$-d_{10}-c obtained using the Bell−Limbach model (see the corresponding solid line in Figure 13).

assumptions had to be made. The dashed line in Figure 6 was calculated as described below.

The master equation for the spin−lattice relaxation rates of nuclei S caused by fluctuations of the heteronuclear dipolar interaction with a spin I exchanging between two sites 1 and 2 has been derived previously.[24] For solids, this equation depends on the molecular orientation with respect to the external magnetic field. However, under MAS conditions in the presence of a two-state tautomeric equilibrium between two forms 1 and 2, the T_1 values are given to a very good approximation by the isotropic average. For H transfer from and to ^{15}N, the relaxation rate of the latter can then be expressed as[21]

$$\frac{1}{T_{1S}^{SI}} = \frac{1}{30}\gamma_S^2\gamma_I^2\hbar^2\left(\frac{\mu_0}{4\pi}\right)^2 I(I+1)R_{SI}\frac{4K_{12}}{(1+K_{12})^2}\times \left[\frac{\tau_c}{1+(\omega_I-\omega_S)^2\tau_c^2}+\frac{3\tau_c}{1+\omega_S^2\tau_c^2}+\frac{6\tau_c}{1+(\omega_I+\omega_S)^2\tau_c^2}\right] \quad (5)$$

where μ_0 is the vacuum permeability, γ_I and γ_S are the gyromagnetic ratios of spins I (hydrogen) and S (nitrogen), respectively, ω_I and ω_S are the corresponding Larmor frequencies, and $\hbar$ is Planck's constant divided by 2π. The inverse of the correlation time τ_c for the tautomerism is given by[21]

$$\frac{1}{\tau_c} = k_{12}+k_{21} = \left(\frac{1+K_{12}}{K_{12}}\right)k_{12} \quad (6)$$

and the geometric factor R_{SI} resulting from the dipolar interaction between the two spins is

$$R_{SI} = r_{SI1}^{-6} + r_{SI2}^{-6} + r_{SI1}^{-3}r_{SI2}^{-3}(1-3\cos^2\alpha) \quad (7)$$

where r_{SI1} and r_{SI2} represent the distances between spins S and I in forms 1 and 2, respectively, and α is the jump angle defined in Figure 6a.

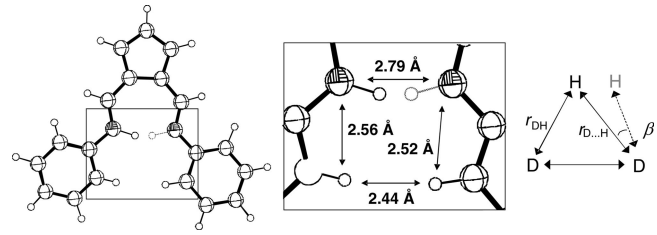

Figure 7. Molecular geometry of **I** in the vicinity of the hydrogen bond according to the X-ray crystallographic structure.[31]

The values of the parameters in eq 5 were evaluated as follows. Parameters with fixed values included the Larmor frequencies $\omega_I = 2\pi \times$ (90.02 MHz) for ^{1}H and $\omega_S = 2\pi \times$ (9.082 MHz) for ^{15}N as well as the corresponding gyromagnetic ratios. The equilibrium constants K_{12} were calculated for each temperature using eq 4. The distances in eq 7 correspond to the short and long distances r_{NH} and $r_{N\cdots H}$ illustrated in Figure 6a, which were assumed to be the same in both tautomers. The jump angle, α, should not be confused with the traditional N−H−N hydrogen bond angle. Pietrzak et al.[28] have proposed the values $r_{NH} = 1.06$ Å and $r_{N\cdots H} = 1.74$ Å along with a N−H−N angle of 170° for **I**; these were derived from the crystallographic distance $r_{NN} = 2.79$ Å[31] and from hydrogen-bond correlations. From these data, the value $\alpha = 5°$ was obtained for the jump angle using trigonometric relations.[21,39] These parameters led to an R_{SI} value of 0.4 Å^{-6}, which was kept constant over the whole temperature range.

In order to calculate the dashed line in Figure 6 using eqs 5 and 6, an Arrhenius law was assumed:

$$k_{12} = A\exp(-E_{a12}/RT) \quad (8)$$

where E_{a12} represents the activation energy of the forward reaction and A is an effective pre-exponential factor. These parameters were adjusted to fit the experimental data in Figure 6b to eq 8; we obtained the values $E_{a12} = 9 \pm 1$ kJ mol^{-1} and $A = 5 \times 10^{12}$ s^{-1}. The expected T_1 minimum was predicted to occur at a temperature of 85 K. Unfortunately, our MAS equipment did not allow us to perform long-time measurements at this temperature.

In a later stage of our studies, we obtained the solid line in Figure 6 using the rate constants for H transfer in crystalline I−$^{15}N_2$-d_{10} calculated using the Bell−Limbach tunneling model (described in the Discussion). In fact, a very large flat minimum is predicted by these data; unfortunately, we could not verify this because of our experimental limitations.

^{2}H NMR Spectroscopy and Longitudinal Relaxation of Static Samples of Ring-Deuterated Polycrystalline and Amorphous I-$^{15}N_2$-d_{10}. As ^{2}H NMR experiments on static powdered samples can be performed at cryogenic temperatures, we wondered whether it would be possible to obtain information about the H transfer rates in **I** using this method. This was indeed the case, as described in this section.

The X-ray structure of **I** indicates that the distances between the mobile proton and the nearest aromatic protons are on the order of only 2.5 Å, as indicated in Figure 7. Therefore, we anticipated that deuterons at these nearest aromatic sites would be relaxed by the mobile hydrogen via dipolar interactions, whereas deuterons at more distant sites should not experience this kind of relaxation. As it is not possible to deuterate only the nearest aromatic proton sites, we performed measurements on the isotopologue in which the aromatic rings are fully deuterated, assuming that in the case of dipolar relaxation, the

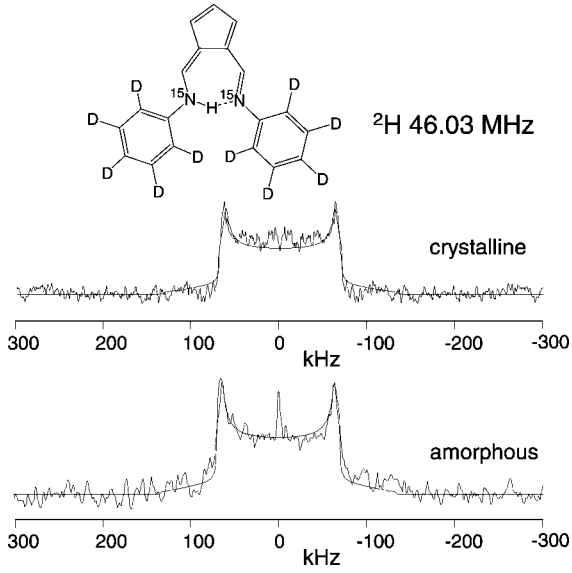

Figure 8. Superimposed experimental and simulated room-temperature ^{2}H NMR spectra of static samples of **I**-^{15}N$_2$-d_{10}-c and **I**-^{15}N$_2$-d_{10}-a measured at 46.03 MHz (7 T).

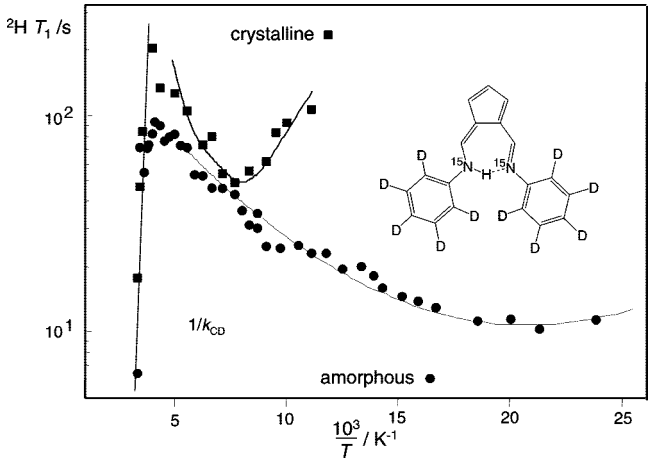

Figure 9. ^{2}H longitudinal relaxation times T_1 for static samples of crystalline **I**-^{15}N$_2$-d_{10}-c and amorphous **I**-^{15}N$_2$-d_{10}-a measured at 7 T, plotted as functions of reciprocal temperature. The solid lines were calculated as described in the text.

observed signal should stem entirely from the nearest deuterons. However, a dipolar relaxation mechanism can be only observed in the absence of quadrupolar ^{2}H relaxation. We will show below that in the case of **I**, such a quadrupolar mechanism is operative only at high temperatures, as it requires major molecular motions or ring flips.

Experimental room-temperature ^{2}H NMR spectra of **I**-^{15}N$_2$-d_{10}-c and **I**-^{15}N$_2$-d_{10}-a (recorded as described in the Experimental Section, using recycle delays of 10 s) and superimposed simulated spectra are depicted in Figure 8. From the simulation of these spectra, quadrupole coupling constant (q_{cc}) values of 171 and 172 kHz and asymmetry factors (η) of 0.08 and 0.07 were obtained for **I**-^{15}N$_2$-d_{10}-c and **I**-^{15}N$_2$-d_{10}-a, respectively. These parameter values indicate that fast phenyl-group flips are absent; such flips would correspond to 120° jumps in the quadrupole coupling tensors and lead to typical line-shape changes as discussed in the next section (see the $K_{12} = 1$, $\theta =$ 120° case in Figure 10). The values of q_{cc} are slightly smaller than the 180−185 kHz values usually observed for immobile

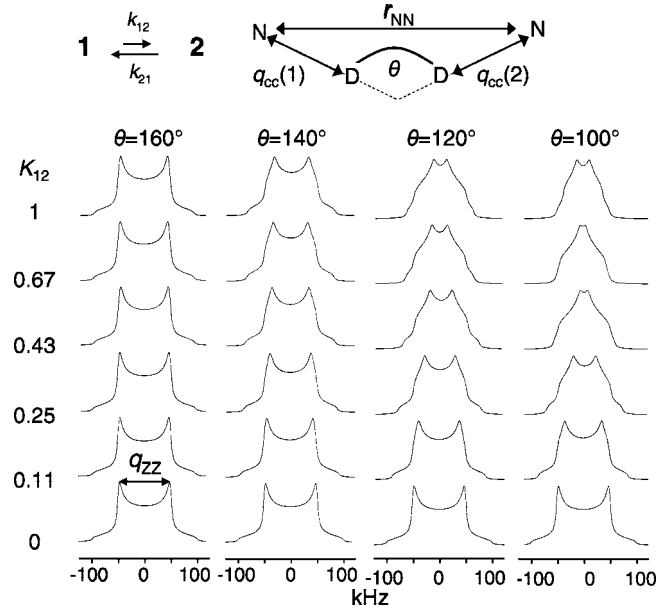

Figure 10. Calculated ^{2}H NMR spectra of a powdered sample containing deuterons exchanging rapidly between two states 1 and 2. The quadrupole coupling constants $q_{cc}(1)$ and $q_{cc}(2)$ of the two tautomeric states were both set to a value of 133 kHz. The intrinsic asymmetry factors were set to zero. The parameters varied were the equilibrium constant for the exchange, K_{12}, and the jump angle of the deuteron quadrupole coupling tensor, θ. Additional details about the calculations are provided in the text.

aromatic deuterons.[40,41] Such a reduction could arise from small-angle motions of the phenyl rings or the whole molecule; however, this question was not studied further.

While the line shapes did not change when the temperature was decreased, substantial changes in the ^{2}H NMR longitudinal relaxation times (measured using the saturation−recovery technique) were observed. Within the margin of error, the magnetization recovery curves were found to be single exponentials.

The ^{2}H T_1 times obtained for **I**-^{15}N$_2$-d_{10}-c and **I**-^{15}N$_2$-d_{10}-a are included in Table S3 in the Supporting Information and plotted as a function of reciprocal temperature in Figure 9. A ^{2}H T_1 maximum at 250 K was observed for each form, beyond which the T_1 values decreased rapidly with increasing temperature. We attribute this finding to the onset of quadrupole relaxation caused by ring flips. As the temperature decreased, the T_1 values of the crystalline form decreased, reaching a minimum of 50 s at 130 K, and then increased again. In contrast, the values of the amorphous form continued to decrease, reaching a flat minimum at 50 K.

In order to analyze the data, we assumed that the relaxation rate of the quadrupole nucleus S (=^{2}H) is given by a sum of two terms:

$$\frac{1}{T_{1S}} = \frac{1}{T_{1S}^{Q}} + \frac{1}{T_{1S}^{IS}} \tag{9}$$

where T_{1S}^{Q} represents the quadrupole relaxation mechanism arising from reorientations of the C_6D_5 groups (CD reorientation) and T_{1S}^{IS} the ^{2}H dipolar relaxation mechanism caused by the mobile proton I (=^{1}H) in the hydrogen bond. Since it has been

(40) Gedat, E.; Schreiber, A.; Findenegg, G. H.; Limbach, H.-H.; Buntkowsky, G. *J. Phys. Chem. B* **2002**, *106*, 1977–1984.
(41) Parker, W. O., Jr.; Hobley, J.; Malatesta, V. *J. Phys. Chem. A* **2002**, *106*, 4028–4031.

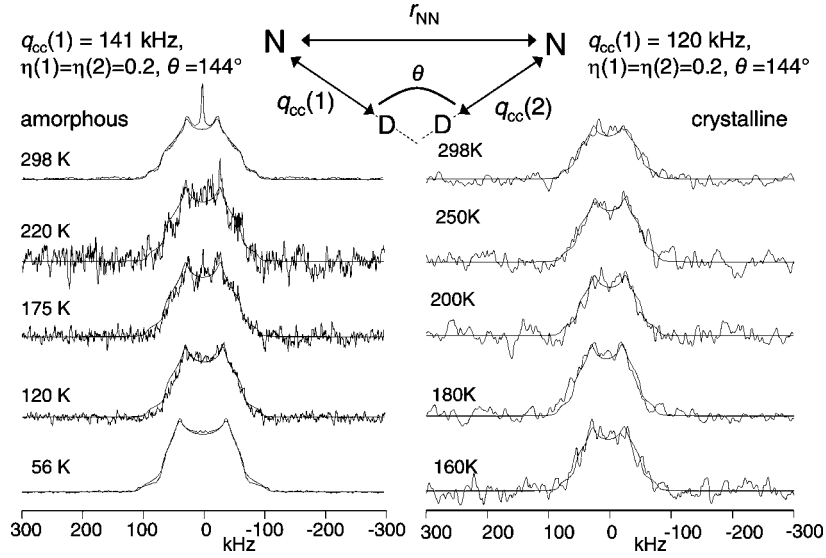

Figure 11. Superimposed experimental and calculated ^{2}H NMR spectra of static samples of amorphous and crystalline **I**-$^{15}N_2$-d_1 measured at 46.03 MHz (7 T).

shown[21] that the dependence of T_{1S}^{IS} on the crystallite orientation in static powdered samples is small, we assumed that eqs 5–7 were also applicable for describing the ^{2}H relaxation caused by modulation of the dipolar ^{1}H−^{2}H interaction in the presence of the proton tautomerism in static samples of **I**-$^{15}N_2$-d_{10}-c and **I**-$^{15}N_2$-d_{10}-a.

As we did not analyze the CD reorientation in more detail, we expressed the first term in eq 9 using the Arrhenius law

$$\frac{1}{T_{1S}^{Q}} = \frac{1}{T_{1S}^{Q}(T_0)} \exp\left[-\frac{E_{CD}}{R}\left(\frac{1}{T} - \frac{1}{T_0}\right)\right] \qquad (10)$$

giving rise to the solid line on the left-hand side of Figure 9. We found values of 45 kJ mol^{-1} and 0.5 s for E_{CD}, the activation energy for CD reorientation, and T_{1S}^{Q}(298 K), respectively. As the spectra at room temperature did not indicate fast 180° ring flips, we assigned this process to a reorientation of the whole molecule at high temperatures that possibly was coupled to molecular diffusion processes involving crystal defects. In other words, the quadrupolar relaxation term dominates only for $T >$ 200 K and can be neglected below this temperature. Moreover, the values of T_1 measured below 200 K were not averaged by 180° phenyl flips, i.e., they correspond to the relaxation times T_{1S}^{IS} arising from the modulation of the dipolar interaction between the mobile H and the nearest aromatic deuterons. This is plausible because the quadrupole relaxation is not efficient at low temperatures and spin diffusion among aromatic deuterons of static powdered organic solids is poor.[42]

From an initial data analysis in the neighborhood of the two T_1 minima using eq 5 and assuming simple Arrhenius laws, we obtained geometrical factors R_{SI} of 0.006 and 0.13 Å^{-6} for the crystalline and amorphous samples, respectively. Assuming that these values would show little dependence on temperature, in the next step we converted the experimental ^{2}H T_1 values into rate constants k_{12} using a homemade computer program based on eqs 4 and 5. The rate constant values obtained in this way are included in Table S3 in the Supporting Information. These data were then assembled in an Arrhenius diagram, which revealed non-Arrhenius behavior that was simulated using the Bell−Limbach tunneling model, as described in the Discussion. Finally, the calculated rate constants were reconverted back into T_1 values, yielding the solid lines in the right-hand portion of Figure 9, which provide excellent fits of the experimental data.

^{2}H NMR Spectroscopy and Longitudinal Relaxation of Crystalline and Amorphous I-$^{15}N_2$-d_1. In order to determine H/D KIEs on the proton tautomerism of **I** in the crystalline and amorphous phases, we performed ^{2}H NMR measurements on samples deuterated only at the mobile proton sites. In contrast to the aromatic deuterons, the two-site deuteron tautomerism affects the ^{2}H NMR line shapes. Spectra calculated using the computer program NMR WebLab 4.1.2 written by Spiess et *al.*[43] are shown in Figure 10. The simulations were performed using a natural line width W_0 given by the expression $W_0 = (\pi T_2)^{-1} = (0.05s\pi)^{-1} = 6.37$ Hz. It was assumed that both sites exhibit the same intrinsic axially symmetric quadrupole coupling tensors: $q_{cc}(1) = q_{cc}(2) = q_{cc} = 4q_{zz}/3$, where q_{zz} was set to a value of 100 kHz. Setting $K_{12} = 0$ gave typical Pake doublets, in which the two maxima are separated by q_{zz}. Increasing K_{12} to a value of 1 led to line-shape changes that depended on the value of θ, the jump angle defined at the top of Figure 10. For $\theta = 180°$, no changes occurred, but as the angle was decreased, the two maxima shifted toward each other. For $\theta = 90°$ and $K_{12} = 1$, q_{cc} was reduced to half the original value, exhibiting an effective value of zero for the asymmetry factor, η.

Figure 11 displays superimposed experimental and calculated ^{2}H NMR spectra of **I**-$^{15}N_2$-d_1-a and of **I**-$^{15}N_2$-d_1-c obtained at 46.03 MHz. In contrast to the results at lower temperatures, the signal-to-noise ratio (SNR) of the room temperature spectrum of **I**-$^{15}N_2$-d_1-a was excellent, as very long measuring times were possible. However, because the ^{2}H T_1 values decreased as the temperature was decreased, the SNR improved again. In contrast, the ^{2}H T_1 values of **I**-$^{15}N_2$-d_1-c were larger; moreover, the spectra stemmed from a series of ^{2}H T_1 measurements using the saturation−recovery technique, which limited the total measuring time and hence the SNR.

(42) Gan, Z.; Robyr, P.; Ernst, R. R. *Chem. Phys. Lett.* **1998**, *283*, 262–268.

(43) Macho, V.; Brombacher, L.; Spiess, H. W. *Appl. Magn. Reson.* **2001**, *20*, 405–432.

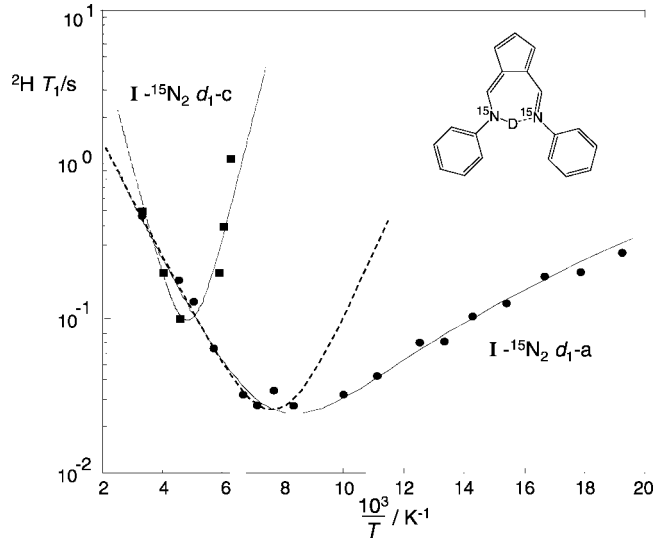

Figure 12. Longitudinal ^{2}H T_1 relaxation times for static samples of polycrystalline **I**-^{15}N$_2$-d_1-c and amorphous **I**-^{15}N$_2$-d_1-a measured at 46.03 MHz (7 T), plotted as a function of reciprocal temperature. The solid lines were calculated as described in the text.

In order to simulate the spectra, the equilibrium constants were taken from eq 4. The remaining parameter values (q_{cc} = 120 kHz, $\eta = 0.2$, and $\theta = 144°$) were optimized and kept constant for all of the spectra. The agreement between the simulated and experimental spectra was very satisfactory in the case of **I**-^{15}N$_2$-d_1-a. For **I**-^{15}N$_2$-d_1-c, the same parameters were applied, but the fit was less satisfactory. Thus, the poor SNR did not allow us to elucidate possible changes in q_{cc}, η, or θ in the crystalline form.

Results of T_1 measurements performed using the saturation−recovery technique are given in Table S3 in the Supporting Information and depicted in Figure 12 as a function of reciprocal temperature. T_1 minima were observed at 220 K for the crystalline form and 120 K for the amorphous form.

To fit these data, we proceeded in a manner similar to that described above. The master equation for the relaxation of a deuteron (spin I) in a hydrogen bond can be expressed in the following form:[44]

$$\frac{1}{T_{1I}} = \frac{3\pi^2 C}{10}\frac{K_{12}}{(1+K_{12})^2}\left(\frac{\tau_c}{1+\omega_I^2\tau_c^2} + \frac{4\tau_c}{1+4\omega_I^2\tau_c^2}\right) \quad (11)$$

The equilibrium constants K_{12} were taken from eq 4. From an initial data analysis in the neighborhood of the T_1 minimum using an Arrhenius law for k_{12}, we obtained C values of 2.1×10^9 and 1.7×10^{10} s^{-2} for the crystalline and amorphous forms, respectively. Assuming that these values would show little dependence on temperature, in the next step we converted the experimental ^{2}H T_1 values into k_{12} values using a homemade computer program based on eqs 4 and 11. The rate constants obtained in this way are included in Table S3 in the Supporting Information. These data were then assembled in an Arrhenius diagram. As before, this diagram revealed non-Arrhenius behavior that was simulated using the Bell−Limbach tunneling model, as described in the Discussion. Finally, the calculated rate constants were converted back into T_1 values, yielding the solid lines in the right-hand portion of Figure 12, which fit the experimental data very well.

Discussion

Using ^{15}N solid-state NMR, we have detected fast quasidegenerate tautomerism between two tautomeric states (1 and 2 in Figure 1a) in polycrystalline and amorphous **I**. In contrast, no tautomerism was observed for solid **II**. In the amorphous form of **I**, the tautomerism was much faster than in the crystalline form. The spectra showed that the gas-phase and solution degeneracy of the tautomerism in **I** is lifted in the solid state by intermolecular interactions. From the dependence of the ^{15}N chemical shifts on temperature, the associated equilibrium constants K_{12} could be obtained. Whereas in the crystalline form, all of the molecules exhibit the same equilibrium constant for tautomerism, a distribution of equilibrium constant values was observed for the amorphous form. Similar environmental effects on the thermodynamics and kinetics of a solid-state proton tautomerism have been observed previously for phthalocyanine.[38] There, the tautomerism was much faster in the β form than in the α form. Moreover, a distribution of equilibrium constant values was observed for an amorphous form.

Information about the kinetics (including H/D KIEs) of the ultrafast tautomerism on the microsecond-to-nanosecond time scale was obtained over a wide temperature range using a combination of longitudinal ^{15}N and ^{2}H T_1 relaxation time measurements on isotopically labeled **I** and appropriate data analyses. In what follows, the results of these measurements are discussed in detail.

Molecular Geometries in the Crystalline and Amorphous Phases of I. The crystal structure of **I** is depicted in Figure 1b. All of the atoms of the fulvenealdimine skeleton, including the atoms of the N−H−N hydrogen bond, are located in a single plane. The N···N distance is $r_{NN} = 2.79$ Å.[31] The position of the hydrogen atom cannot be determined by X-ray diffraction, but on the basis of hydrogen-bond correlations, Pietrzak et al.[28] have proposed values of $r_{NH} = 1.06$ Å and $r_{N\cdots H} = 1.74$ Å along with a N−H−N hydrogen-bond angle of 170°. The phenyl rings are not located in the molecular plane: the valence-bond and torsional angles at the amino nitrogen are $\alpha_1 = 124.1°$ and $\phi_1 = 7°$, while those at the imino nitrogen are $\alpha_2 = 121.0°$ and $\phi_2 = 21.6°$ (Figure 1b). It is obvious that the different geometries around the two nitrogen atoms, which are fixed by the molecular environment, contribute to the loss of the gas-phase degeneracy of the tautomerism of **I**. A similar phenomenon has been observed recently for the double proton transfer in bis(arylformamidine) dimers,[19,45] where it was found that having similar torsional angles at the two nitrogen atoms ($\phi_1 \approx \phi_2 \approx 30°$) is optimal for proton transfer. We note, however, that H transfer in **I** is not quenched by the different conformations of the phenyl rings. Thus, the latter have a smaller effect on the basicity of the attached nitrogen atoms than chemically different rings, such as the phenyl and triazole rings in **II**, which does not exhibit any sign of tautomerism.

The ^{15}N spectra of the amorphous phase of **I** shown in Figure 5 indicate a distribution of equilibrium constant values, as observed previously for amorphous phthalocyanine[38] and for a six-membered N−H−N chelate in polystyrene.[37] However, the average equilibrium constant value is similar to that of the

(44) Medycki, W. R.; Reynhardt, E. C.; Latanowicz, L. *Mol. Phys.* **1998**, *93*, 323–328.

(45) Anulewicz, R.; Wawer, I.; Krygowski, T. M.; Männle, F.; Limbach, H.-H. *J. Am. Chem. Soc.* **1997**, *119*, 12223–12230.

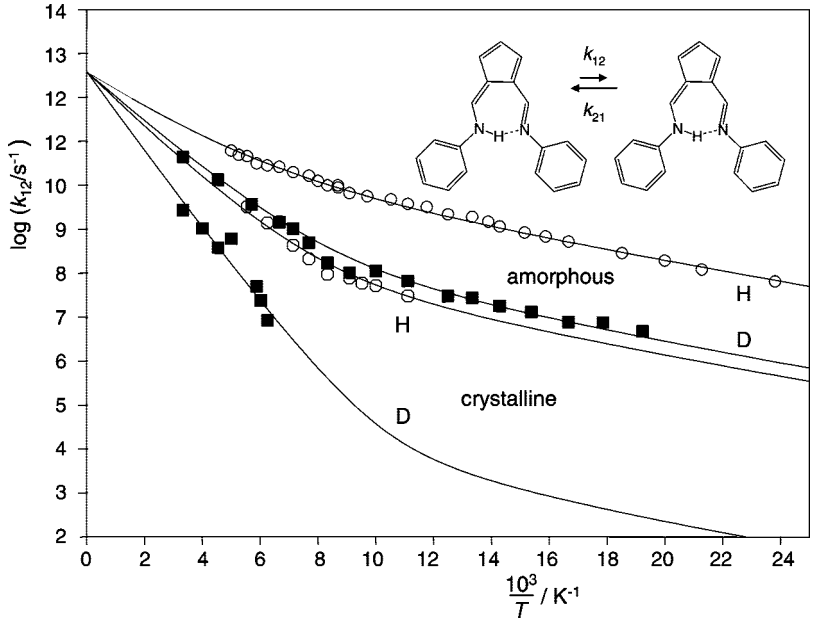

Figure 13. Arrhenius curves for solid-state tautomerism in polycrystalline and amorphous isotopically labeled **I**. The upper two curves are for the amorphous form and the lower two curves for the polycrystalline form; in each pair of curves, ○ and ■ represent data for H and D transfer, respectively. The solid lines were obtained by fitting the experimental data using the Bell−Limbach tunneling model with the parameter values given in Table 2.

crystalline form, which was also present and whose fraction slowly increased with time.

Longitudinal Relaxation and H-Transfer Kinetics of I in the Solid State. In a first attempt, we tried to determine the inverse correlation times $\tau_c^{-1} = k_{12} + k_{21}$ and, using the known values of $K_{12} = k_{12}/k_{21}$, the rate constants k_{12} for the solid-state tautomerism of **I** by measuring ^{15}N T_1 values of **I**-$^{15}N_2$ at 9.12 MHz. At this frequency, these values are governed by modulation of the dipolar ^{1}H−^{15}N interaction induced by the proton transfer rather than by the ^{15}N chemical shift anisotropy.[21] In various cases studied previously, where slower proton transfers were studied, ^{15}N T_1 minima were obtained at low temperatures; these made possible the conversion of ^{15}N T_1 values into rate constant values.[19,21,22] In contrast, in the case of **I**-$^{15}N_2$, the ^{15}N T_1 values decreased as the temperature was decreased, but a minimum could not be reached (Figure 6) because the H-transfer process is too fast.

Therefore, we probed the H transfer in crystalline and amorphous **I** by measuring ^{2}H T_1 values of static samples. Only at high temperatures molecular motions were a source for quadrupole relaxation, leading to similar ^{2}H T_1 values for the crystalline and amorphous forms that decreased with increasing temperature (left-hand side of Figure 9), corresponding to an activation energy of 45 kJ mol^{-1}. However, at lower temperatures, the relaxation curves of both phases of **I** exhibited a second relaxation mechanism that produced T_1 minima. We attributed these findings to modulation of the dipolar interactions with ring deuterons located near the mobile H in the N−H−N hydrogen bond. For comparison, we also measured ^{2}H T_1 values for crystalline and amorphous forms of **I** that were deuterated at the hydrogen bond but not at the aromatic rings (Figure 12). The mobile D was relaxed by a quadrupole relaxation mechanism.

A T_1 minimum indicates the presence of a dynamic process exhibiting an inverse correlation time τ_c^{-1} close to the Larmor frequency of 46 MHz, independent of the operative relaxation mechanism. For the crystalline form, the minimum caused by the H transfer was observed at 130 K (Figure 9) and that caused by the D transfer at 220 K (Figure 12), indicating a large H/D KIE. The rate constants and KIEs were even larger for the amorphous form, where the H and D transfers led to flat minima at 50 and 120 K, respectively. The observation of these KIEs does indeed provide evidence that the aforementioned interpretation of a dipolar ^{1}H−^{2}H relaxation mechanism for the ring-deuterated phases is correct. Since we could observe the minima, we were also able to obtain the constants R_{HD} (R_{SI} in eq 5, with S = H and I = D) and C (eq 11) from the ^{2}H T_1 values at the minima. These parameters respectively describe the modulation of the dipolar coupling tensor of the ring deuterons with the jumping H and the modulation of the quadrupole coupling tensor of a jumping D. Assuming these constants to be temperature-independent, we were able to convert the T_1 values into k_{12} values for H and D transfer (as described above) using the K_{12} values determined using ^{15}N NMR, which are isotope-independent.

Not only the values of the rate constants but also the values of the constants R_{SI} and C were substantially smaller for the crystalline phases than for the amorphous phases. R_{SI} can be calculated using eq 7. If it is assumed that the H−D distances are the same in the two tautomeric forms 1 and 2 (i.e., if $r_{HD1} = r_{HD2} \equiv r_{HD}$), it follows that

$$R_{HD} = 3r_{HD}^{-6}(1 - \cos^2 \alpha) \qquad (12)$$

The factor C can be approximated in a similar way.[44] If it is assumed that the quadrupole coupling tensors q_{cc} are the same in both tautomeric forms, it follows that

$$C = 3q_{cc}^2(1 - \cos^2 \theta) \qquad (13)$$

Thus, the different values of these factors for the crystalline and the amorphous forms can arise from different values of r_{HD} and C and/or from different jump angles. In order to obtain more information about this problem, at least in the case of C, we performed line-shape analyses of the jumping deuterons (Figure 11). We observed a quadrupole coupling constant of $q_{zz} = 3q_{cc}/4 = 106$ kHz for the amorphous forms. In contrast, we found a smaller coupling constant (90 kHz) for the crystalline

Table 2. Geometric and Kinetic Data and Arrhenius-Curve Simulation Parameters for Solid-State Tautomerism of **I** and Related Systems

	ref	r_1 (Å)	r_2 (Å)	q_1 (Å)	q_2 (Å)	r_{NN} (Å)	$k^H_{12,298K}$ (s^{-1})	$(k^H_{12}/k^D_{12})_{298K}$	E_m (kJ mol^{-1})	log(A/s^{-1})	E_d (kJ mol^{-1})	Δm (amu)	2a (Å)	$\Delta\varepsilon$ (kJ mol^{-1})
crystalline **I**[a]	this work	1.06	1.74	0.34	2.80	2.79	−	9	2.1	12.6	10.2	1	0.66	5.2
amorphous **I**[b]	this work	1.08	1.68	0.30	2.76	−	−	4	2.1	12.6	5.9	1.5	0.40	3.1
III[c]	50	1.03	2.31	0.64	3.34	−	10^5	16	10.0	12.6	34.3	0	0.87	6.5
III‡ [d]	50	1.33	1.33	0.005	2.66	−	−	−	−	−	−	−	−	−
IV	22	1.03	1.94	0.45	2.97	2.97	3×10^9	−	3.4	12.6	15.1	3	0.17	1.05

[a] Geometries from ref 28; all other data from this work. [b] This work; geometries from Figure 14. [c] Data from refs 7 and 20. [d] Calculated transition-state values from refs 7 and 22.

form. This finding indicates that the deuteron in the hydrogen bond exhibits shorter relaxation times in the amorphous form than in the crystalline form. This difference must arise from slightly different H-bond geometries in the two phases. It is then also plausible that the dipolar $^1H-^2H$ relaxation is more efficient in the amorphous form. It would have been desirable to obtain further information about the H-bond structures from these data. However, this would have required extended theoretical calculations that were beyond the scope of the present study.

Simulation of Arrhenius Curves. We finally arrive at the discussion of the Arrhenius curves for H and D transfers in the crystalline and amorphous phases of **I**. The rate constants we obtained are assembled in the Arrhenius diagram shown in Figure 13. We observe from this figure that H transfer was substantially faster in the amorphous form than in the crystalline form. Also, non-Arrhenius behavior typical of tunneling is observed. While the KIEs are temperature-dependent at high temperatures, they are temperature-independent at low temperatures for the amorphous form, implying that the Arrhenius curves should be parallel. The H/D KIE had a value of 4 at 298 K for the amorphous form but seemed to be substantially larger (9) for the crystalline form. These KIE values are smaller than the value of 16.5 found for tautomerism of the porphyrin anion[20] but similar to the HH/HD KIEs of various double proton transfers in cyclic dimers of pyrazoles[18] and amidines.[19]

The solid Arrhenius curves were calculated using the Bell tunneling model[3] as modified by Limbach.[5,7] This model provides a first screening of kinetic data for anomalies such as pre-equilibria, unusual frequency factors, and mismatches of KIEs at low and high temperatures. Moreover, it provides a platform for the discussion of different molecular systems and processes. On the other hand, it does not preclude more in-depth theoretical analyses that can give definitive answers about the reaction mechanisms.[15]

The parameter values used to calculate the solid Arrhenius curves in Figure 13 are assembled in Table 2. A common pre-exponential factor of $A = 10^{12.6}$ s^{-1} was used for all of the processes. E_m represents a minimum energy for tunneling to occur. Its value is isotope-insensitive and determines the slope of the Arrhenius curve at low temperatures. For a single H transfer in the absence of pre-equilibria, E_m corresponds to a reorganization energy for compressing the N···N distance. Only in a compressed configuration can tunneling occur.[46] Such a two-stage process was found for the porphyrin tautomerism by means of ab initio calculations.[47] $E_d^H \equiv E_d$ represents the intrinsic barrier for H transfer at the geometry where tunneling becomes operative. The intrinsic barrier for D transfer is given by $E_d^D = E_d + \Delta\varepsilon$, where $\Delta\varepsilon$ is determined primarily by the difference in zero-point energies of the initial and transition states. Another parameter is the barrier width 2a, which represents the base of an inverted parabola. Finally, in contrast to the Bell model, where the tunneling masses of H and D are 1 and 2 amu, respectively, it is assumed that these masses are given by $m^H = 1 + \Delta m$ and $m^D = 2 + \Delta m$, respectively, where Δm takes into account small heavy-atom displacements during the tunneling process. Effectively, an increase in Δm decreases the KIE in the low-temperature regime.

The curve simulation parameters in Table 2 were derived as follows. We first simulated the Arrhenius curves of the amorphous form, which gave the better data set. We found that a common value of $A = 10^{12.6}$ s^{-1} for the pre-exponential factors of all of the isotopic reactions could well describe all of the experimental data. E_m was determined from the slopes at low temperatures. Then, E_d and $\Delta\varepsilon$ were determined from the slopes of the Arrhenius curves at high temperatures. Finally, Δm and 2a were adjusted to fit the rate constants and KIEs at low temperatures. In the case of the crystalline form, the kinetic data were more scattered and incomplete, especially at low temperatures. Therefore, as an approximation, we assumed values of E_m and Δm similar to those in the amorphous form. In contrast, $E_m + E_d$ and $\Delta\varepsilon$ could be determined from the high-temperature values; both were significantly larger than in the amorphous form. This left 2a as the only adjustable parameter for fitting the non-Arrhenius character of the curves. We had to use a substantially larger value, which is consistent with a larger barrier height, E_d.

Geometries and Barriers for H Transfer in Intramolecular N−H−N Hydrogen Bonds. In order to discuss these results in a wider context, we have included in Table 2 some geometric and kinetic data for **I** and related degenerate or near-degenerate intramolecular N−H−N transfers studied previously, namely, those in porphyrin anion (**III**)[20] and polycrystalline tetramethyldibenzotetraaza[14]annulene (**IV**).[22]

We also refer to N−H−N hydrogen-bond correlations in Figure 14a, where the heavy-atom coordinates $q_2 = r_1 + r_2$ are depicted as a function of the proton hydrogen bond coordinates $q_1 = {}^1/_2(r_1 - r_2)$. For a linear H bond, q_1 represents the distance of the proton from the H-bond center and q_2 the distance between the heavy atoms. As several papers have shown on the basis of neutron-diffraction studies, these two coordinates are correlated.[7,48,49] The solid line corresponds to equilibrium structures as calculated by ab initio methods. The dotted line includes an empirical correction for quantum zero-point vibrations of the H-bonded proton. We have included data points for **I**−**IV** derived as follows. Data for **III** were taken from ab

(46) Scherer, G.; Limbach, H.-H. *J. Am. Chem. Soc.* **1994**, *116*, 1230–1239.
(47) Maity, D. K.; Bell, R. L.; Truong, T. N. *J. Am. Chem. Soc.* **2000**, *122*, 897–906.
(48) Limbach, H.-H.; Pietrzak, M.; Benedict, H.; Tolstoy, P. M.; Golubev, N. S.; Denisov, G. S. *J. Mol. Struct.* **2004**, *706*, 115–119.
(49) Limbach H.-H.; Denisov, G. S.; Golubev, N. S. In *Isotope Effects in Chemistry and Biology*; Kohen, A., Limbach, H.-H. Eds.; Taylor & Francis: Boca Raton, FL, 2006; Chapter 7, pp 193−230.

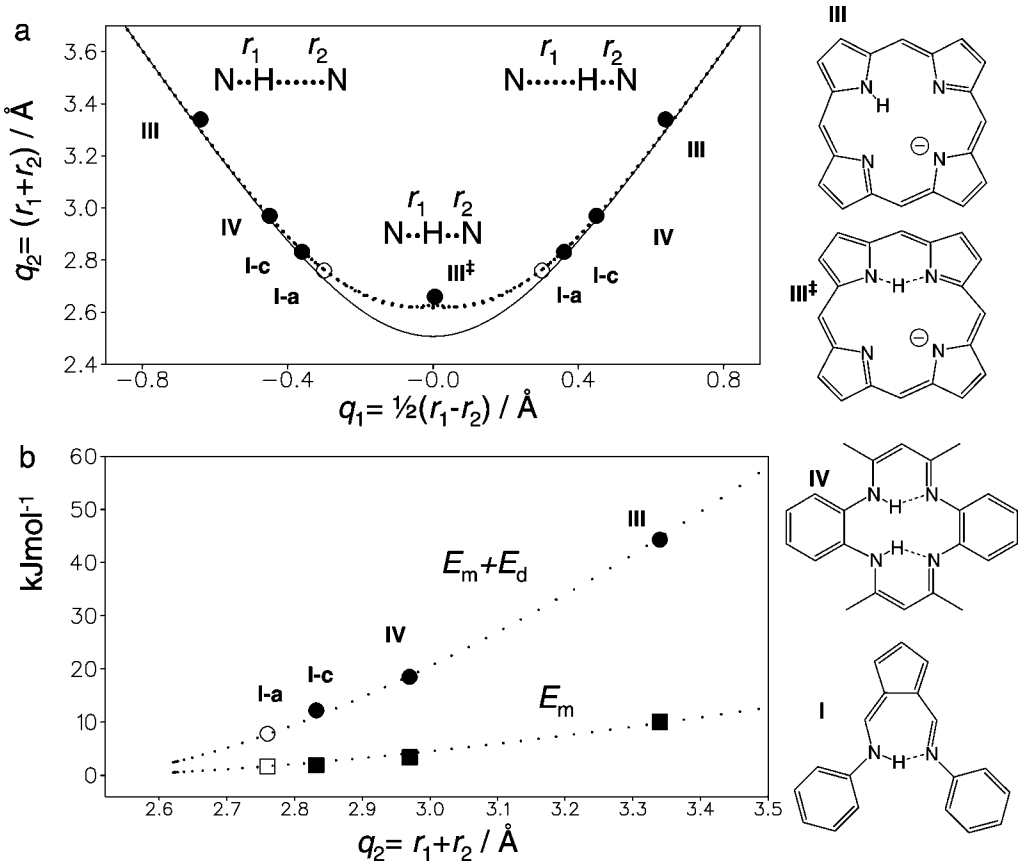

Figure 14. (a) H-bond geometries of various molecular systems containing N−H−N hydrogen bonds. (b) Total barrier heights ($E_d + E_m$) and minimum energies for tunneling (E_m) for the H transfers in the species in (a), as calculated from the Arrhenius curves (see Table 2 and the text).

initio calculations[50] and data for **IV** from the X-ray crystal structure and dipolar N−D couplings.[22,51] The data point for crystalline **I** was derived from the crystallographic N···N distance for a hydrogen-bond angle of 160° derived from ab initio calculations.[27,28] In all cases it was assumed that the geometric hydrogen-bond correlation is fulfilled. Therefore, all of the data points are located on the dotted correlation curve. We have included the ab initio geometry of the porphyrin anion transition state (**III**‡) at $q_1 = 0$, for which $q_2 = 2.66$ Å.[50] This value is close to that in the geometry of the strongest symmetric N−H−N hydrogen bond (2.52 Å) at normal pressures.

The graph of Figure 14a indicates that the minimum-energy path for a degenerate H transfer in a N−H−N hydrogen bond must involve an important hydrogen-bond compression, as we have argued in a number of papers.[5,7,23,46,52] Such a compression does not involve large H/D KIEs and is responsible for the reorganization energy E_m preceding the H transfer, as discussed above. The compression takes place preferentially along the correlation line until the system reaches a configuration (at a given value of q_2) where H is transferred from the left to the right side of the correlation curve, going through the transition state at $q_1 = 0$. Here, tunneling and zero-point energy changes along the minimum-energy path dominate the overall H/D KIEs. We note that evidence for such a two-stage process has been found in ab initio calculations of porphyrin.[47]

The question of whether $E_m + E_d$ and E_m are related to the hydrogen-bond geometries of the initial states now arises. Support for this statement comes from Figure 14b, where the experimental values of both quantities (solid symbols) are plotted as a function of q_2. Indeed, we found the correlation illustrated by the dotted line, which was calculated using the expressions

$$E_d + E_m = \kappa(q_2 - q_{2min})^{1.5} \qquad E_m = 0.22(E_d + E_m) \tag{14}$$

where $q_{2min} = 2.50$ Å and $\kappa = 58$ kJ mol^{-1} Å^{-1}. It is astonishing that the reorganization energy E_m represents 20% of the total barrier height $E_m + E_d$. Because of the excellent correlation, we were tempted to place the experimental values of $E_m + E_d$ and E_m for amorphous **I** (open symbols) on the dotted lines, from which we estimate that the hydrogen bond in this phase is somewhat stronger than that in the crystalline form (Table 1), as represented by the open symbols in Figure 14a. Thus, in comparison with the crystalline form, the smaller barrier and reorganization energy and the smaller H/D KIEs of the amorphous form of **I** are interpreted in terms of a stronger N−H−N hydrogen bond.

In principle, support for this interpretation could come from a discussion of the quadrupole coupling constant q_{zz} for the hydrogen-bonded deuterons. Generally, when a hydrogen bond is compressed and the deuteron is shifted toward the H-bond center, the value of q_{zz} decreases. Thus, we observed for **IV** a q_{zz} value of 175 kHz,[22] whereas the strong H bonds in crystalline and amorphous **I** studied here exhibited values of only 95 and 106 kHz, respectively. Thus, the smaller value of q_{zz} for crystalline **I** does not support the above interpretation. However,

(50) Vangberg, T.; Ghosh, A. *J. Phys. Chem. B* **1997**, *101*, 1496–1497.
(51) Hoelger, C. G.; Limbach, H.-H. *J. Phys. Chem.* **1994**, *98*, 11803–11810.
(52) Benedict, H.; Limbach, H.-H.; Wehlan, M.; Fehlhammer, W. P.; Golubev, N. S.; Janoschek, R. *J. Am. Chem. Soc.* **1998**, *120*, 2939–2950.

general correlations of q_{zz} and asymmetry factors with H-bond geometries are not presently available, and features other than the latter could play a role.

The discussion of the tunneling parameters Δm and $2a$ is more difficult. These parameters are "soft", and their physical meaning is less well-established than those of $E_m + E_d$ and E_m, which can easily be established at high and low temperatures from the slopes of the Arrhenius curves under favorable conditions. As discussed above, the respective tunneling masses for H and D are not simply 1 and 2 amu but are increased by an amount Δm that takes into account heavy-atom motions during the tunneling process. Clearly, the value of Δm depends on the chemical structure. One could speculate that in the case of **IV**, which has alternating double and single bonds, Δm may be larger than in the aromatic porphyrin anion **III**. The values of the barrier widths $2a$ are on the order expected from the hydrogen-bond geometries. A direct comparison with crystal structure data is difficult, as these values refer to the compressed state in which tunneling can occur and not to the initial states.

Phenyl Group Conformation. Finally, we must discuss the conformation of the phenyl groups of **I**. As illustrated in Figure 1, different conformations, in particular, different valence-bond angles α_1 and α_2 as well as different torsional angles ϕ_1 and ϕ_2, lift the degeneracy of the H transfer. In other words, in the liquid state, the degeneracy of the H transfer requires a reorganization of the phenyl groups, as discussed recently for diarylformamidine dimers.[19] When the conformations of the phenyl groups at the amino and imino nitrogens are very different, only a single tautomeric state can be observed. Thus, part of the reorganization of the initial states into the compressed H-bonded state in which tunneling occurs may also involve some phenyl group reorganization, but it is unlikely that a major reorganization can be achieved in the solid state with similar phenyl group conformations at both nitrogen atoms. Nevertheless, a different phenyl group reorganization could also contribute to the different kinetic behavior of crystalline and amorphous **I**. Thus, it could be the case that the phenyl groups in the latter exhibit a conformation where both the energy necessary for H-bond compression and the barrier for H transfer are reduced compared with those in crystalline **I**, although the H bond might be somewhat stronger in the latter.

Conclusions

Rate constants for the solid-state tautomerism of **I**, including H/D KIEs, were followed in this study by NMR relaxometry on the microsecond-to-picosecond time scale, where the largest rate constants observed were 10^{11} s^{-1}. The Arrhenius curves indicated temperature-dependent isotope effects at high temperatures and temperature-independent ones at low temperatures. The latter observation is explained by a heavy-atom reorganization, namely, a H-bond compression necessary to reach a configuration in which the barrier height is reduced to such an extent that tunneling can occur. A smaller heavy-atom reorganization can occur during the H-tunneling process, reducing the temperature-independent KIEs.

Whereas the tautomerism of porphyrins and the porphyrin anion, which exhibit large barriers, was almost independent of the environment,[20] we have observed a substantial difference in that for amorphous and crystalline **I**, which exhibit quite small barriers for H transfer in the solid state. This observation can imply a difficulty for theoretical calculations, as the effects of different environments must be taken into account when Arrhenius curves calculated using first principles are to be compared with experimental ones. Astonishingly, the KIEs found for **I** were not much smaller than those found for other H transfers exhibiting much larger barriers. Furthergoing studies, e.g., neutron structure determinations and vibrational spectroscopy experiments as well as theoretical studies, are necessary in order to obtain more information about the proton tautomerism of **I**.

Acknowledgment. This work was supported by the Deutsche Forschungsgemeinschaft and the Fonds der Chemischen Industrie, Frankfurt.

Supporting Information Available: ^{15}N chemical shifts for **I**-$^{15}N_2$-c as a function of temperature (Table S1), parameter values for the line-shape simulations of the spectra shown in Figure 5 (Table S2), and longitudinal relaxation times and associated rate constants for H transfer in solid **I**-$^{15}N_2$ and partially deuterated isotopologues (Table S3). This material is available free of charge via the Internet at http://pubs.acs.org.

JA801506N